Protocol for Long-term Electrochemical Tests (CEA)

This protocol has been used to investigate the electrode microstructural evolution upon operation. For this purpose, a set of long-term tests has been performed in the objective to identify the operating parameters affecting the electrochemical degradation.

The experimental set-up is described from the test bench main features to the start-up and shut-down procedures. Then, the electrochemical long-term tests are presented by starting with the initial performances, the selected test conditions for ageing and the degradation rates. The most striking results, which can be inferred from the regular electrochemical measurements carried out on aged cells, are detailed hereafter. Finally, the fine post-mortem characterizations are reported to highlight the effect of the operating parameter on the electrode microstructural evolution.

1. Experimental set-up description

1.1 Test bench

The electrochemical tests have been performed on test bench dedicated to the electrochemical assessment of single button cell. As depicted on Figure 4.1, the test bench presents a radial geometry with a co-flow configuration. The set-up is adapted to operate in fuel cell or electrolysis mode.

The cell housings are made of Crofer22APU without coating. Despite the possible chromium poisoning, the metallic supports present several interesting advantages for the long-term testing. First of all, the metallic set-up is able to withstand thermal cycles without any large cell degradation. More precisely, it has been checked the accumulation of more than 25 thermal cycles does not lead to the fatal cell electrolyte failure or to crack the glass seal. Only a degradation of 2 mV per cycle (measured at 0.5 A/cm², FU=60%) have been found that would be related to a slight electrode deterioration and/or a damage of the electrode current collection [Rinaldi2015]. Furthermore, as shown on Figure 4.1, the metallic housing allows connecting easily the power supply to the set-up. It is worth noting that dry air was used for all the experiments in order to limit the issue related to the Cr release from the metallic interconnect [Fergus2005, Shuler2012]. Indeed, in this condition, the degradation induced by the Cr electrode poisoning over an operating period of more than 2000 hours is expected to be rather negligible [Ghezel2013].

In the test bench, the gas and electrical distributions are ensured by gold and nickel grids of 100 mesh.cm^{-2} at the oxygen and hydrogen electrode sides, respectively. As shown in Figure 4.1, weights corresponding to an applied pressure of 400 g.cm^{-2} have been put for the experiments on the oxygen support to improve the electrical contacts between the grids and the electrodes. The cell voltage is measured by gold wires that are welded on the gold grid or the metallic support for the O_2 and H_2 electrode respectively. The thermal control of the experiment is guaranteed by a thermocouple located close to the cell in the hydrogen gas outlet. A second measurement is done in the furnace near the set-up.

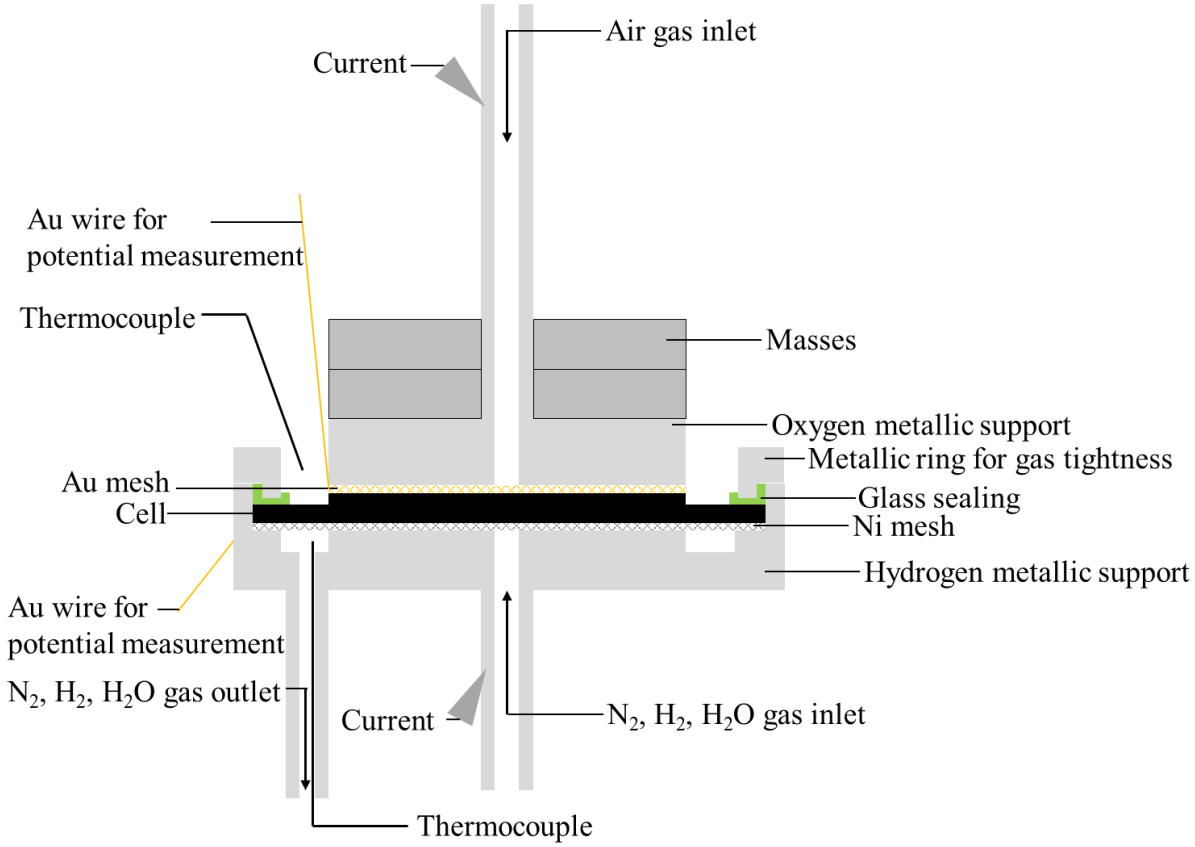

Figure 4.1 – Schematic representation of the experimental set-up near the cell

For both electrodes, the gas are introduced by the centre and are distributed with a radial co-flow configuration on the cell active area of 9.08 cm^2. Mass flow controllers are used for the gas delivery. The oxygen electrode is fed with dry air which is released in the furnace at the exit of the cell. At the hydrogen electrode side, N_2 and H_2 are available for gas distribution. The gas tightness of the hydrogen compartment is ensure by a glass-ceramic seal deposited all around the cell edge. The steam is produced by a bubbler (Figure 4.2) which is a common equipment in literature [Aaberg1998, Park2010, Hauch2011, Zhang2013]. It consists of a porous element inside a metallic container filled of water. The carrier gas is introduced by the bottom of the tank and small bubbles are distributed in the porous element. The proportion of steam in the gas flow is controlled by the humidifier temperature. Thermocouples allow the water and vapour phase's temperatures to be controlled. A pressure sensor is added on the humidifier to follow the inhomogeneity in the steam flow. To limit this effect, a buffer volume is connected to the bubbler (Figure 4.2). The gas inlet pipe is heated up to 110°C until the cell support to avoid water condensation. At the cell outlet, a condenser allows water to be recovered and weighed. The gases are carried away in an air vent.

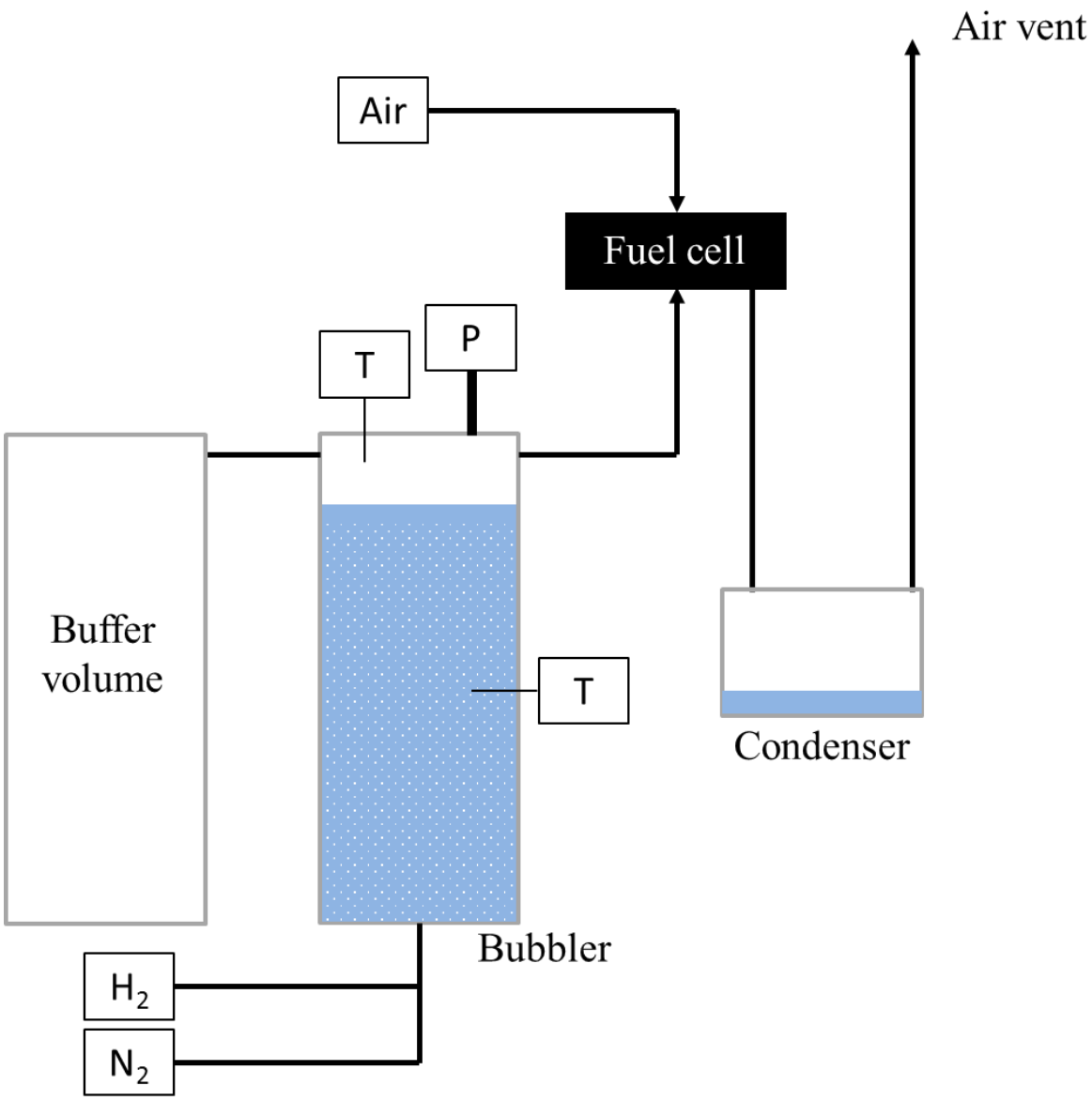

Figure 4.2 – Schematic representation of the complete test bench

On the test bench, the temperature and gas flow rate are driven with the supervision software RSView®. All the data are automatically saved for each seconds. In addition, supervision allows the automation of procedures such as heating, Ni reduction and so on … Security procedures can also be defined in case of alarms.

1.2 Electrochemical performance measurements

Two kinds of measurement have been done to evaluate the cell performances. The first one is the polarisation curve and the second one is the Electrochemical Impedance Spectroscopy (EIS). The specificities related to both the device and the conditions used for the measurements are detailed hereafter.

1.2.1 Polarisation curve

The polarisation curve consists in plotting the current density as a function of the cell potential. A potentiostat/galvanostat (Autolab PGSTAT-302N) equipped with a FRA2 module and a 20 amps current booster has been used during the experiments. The i-U curves have been measured in galvanostatic mode with a sweep rate of 10 or 20 $mA.s^{-1}$. This sweep rate is a good compromise between a fast enough data acquisition and a sufficiently low scanning rate to consider the stationary conditions fulfilled.

1.2.2 Electrochemical Impedance Spectra (EIS)

The EIS is a technique used to separate and identify in the frequency domain the contributions coming from the electrochemical and transport processes occurring in the cell. It is based on the measurement of the system response to a small periodic perturbation in current i or voltage U [Barsoukov2005, Nechache2014]. The cell linear impedance $Z(f)=U/i$ is then evaluated for different frequencies f of the applied signal.

For the tested cells, the data have been recorded in galvanostatic mode. It means that an alternative current perturbation i_{ac} is imposed on the operating direct current density i_{dc}. The cell voltage response is then recorded to evaluate the impedance $Z(f)$. The same device than the one used for the polarisation curve measurements was employed for the EIS acquisition, while the NOVA software was used as interface with the equipment. The half-amplitude in the EIS measurements has been chosen at ±22 $mA.cm^{-2}$ and a frequency range comprised between 10^5 Hz and 10^{-2} Hz has been investigated. One can note that the amplitude of the applied signal was adapted to fulfil the small perturbation assumption in order to obtain a linear response of the system. Before starting the electrochemical characterization, the system was stabilized 2 minutes at the direct current density i_{dc} considered for the EIS data acquisition.

1.3 Start-up and shutdown procedure

The same starting-up procedure has been defined and followed for all the tested cells. The temperature is initially increased to 900°C for the sealing pre-treatment with a rate of $1^{\circ}C.min^{-1}$ to limit the thermal gradient inside the cell. During the heating up, the O_2 and H_2 electrodes are swept under air and nitrogen respectively with flows of 0.5 $NL.h^{-1}$. After 30 minutes at 900°C, the temperature is reduced to 860°C for a 90 minutes step in order to finalise the thermal treatment of the glass seal. The cell is lastly cooled down to 800°C for the next start-up phase.

Before starting the electrochemical experiments, it is required to reduce the nickel oxide of the cermet into its reduced state. This procedure is carried out at 800°C by replacing step by step the nitrogen gas flow by hydrogen according to the protocol given in Figure 4.3. Once under pure hydrogen, the cermet is maintained under this highly reducing condition during 2 hours to complete the full Ni reduction. The cell voltage is usually stabilized after the treatment and can be compared to the expected Open Circuit Voltage (OCV) which is a good indicator of both the full cermet reduction and the gas tightness of the hydrogen compartment. For all the experiments, a difference of less than 8% was obtained between the experimental and theoretical OCV meaning that the Ni contained in the cermet was fully reduced and the H_2 hydrogen compartment was fully gas tight (cf. Table 4.1).

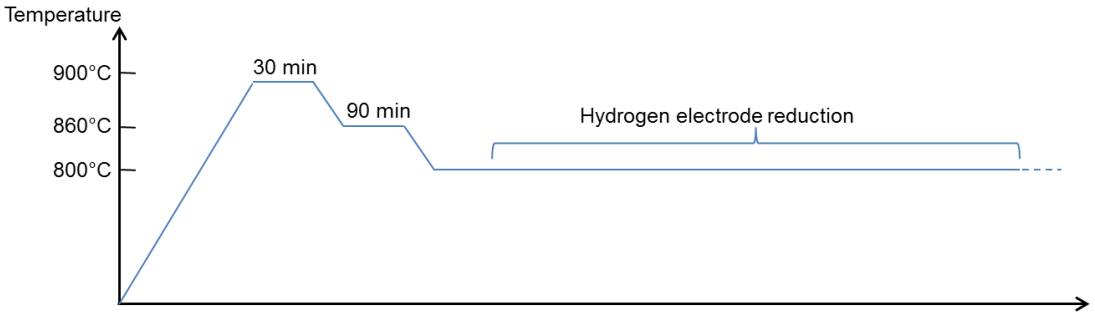

		5 min	5 min	5 min	5 min	5 min	5 min	5 min	90 min
Hydrogen electrode									
N_2 (10^{-6} mol.s^{-1})	6.2	49.6	43.4	37.2	24.8	12.4	0.0	0.0	0.0
H_2 (10^{-6} mol.s^{-1})	0.0	0.0	6.2	12.4	24.8	37.2	49.6	63.6	63.6
Oxygen electrode									
Air (10^{-6} mol.s^{-1})	6.2	49.6	49.6	49.6	49.6	49.6	49.6	63.6	280.1

Figure 4.3 – Starting-up and hydrogen electrode reduction procedures for the cells.

Note that all the experiments were started with the humidifier emptied of water. If steam was required for the durability test, the container was filled with water only after the hydrogen electrode reduction step. The bubbler temperature was then increased to obtain the required ratio of H_2/H_2O.

When the long-term test was completed, the cell was cooled down to room temperature at a rate of -1°C.min^{-1}. Anodic and cathodic gas flows were lowered to 2 NL.h^{-1} by keeping an air sweeping condition for the O_2 electrode whereas a mixture of nitrogen and hydrogen with a N_2/H_2 ratio of 97/3 was used at the hydrogen electrode side. Thanks to this shutdown procedure, all the cells were retrieved without any mechanical damage or oxidation of the cermet. The cells were finally removed from the support by cutting the border with a diamond pen.

2. Electrochemical degradation tests

A series of long-term tests have been performed on the studied cell. The initial performances have been systematically obtained in identical conditions to check the cell reproducibility. The durability test conditions have been selected to highlight the main impacting parameters. The degradation rates are reported in the next section. An analysis of the cell polarisation curves measured during the ageing test is then proposed. Finally, a tentative for a rough analysis of the impedance diagrams is presented.

2.1 Initial performances

The initial performances of the tested cells should be similar as they come from the same manufacturing batch. For all the tested cell, a polarisation curve was recorded at 800°C under dry hydrogen and air. The gas flows were 3.16NL.h^{-1} and 22.6 NL.h^{-1} at the H_2 and O_2 electrode respectively. In

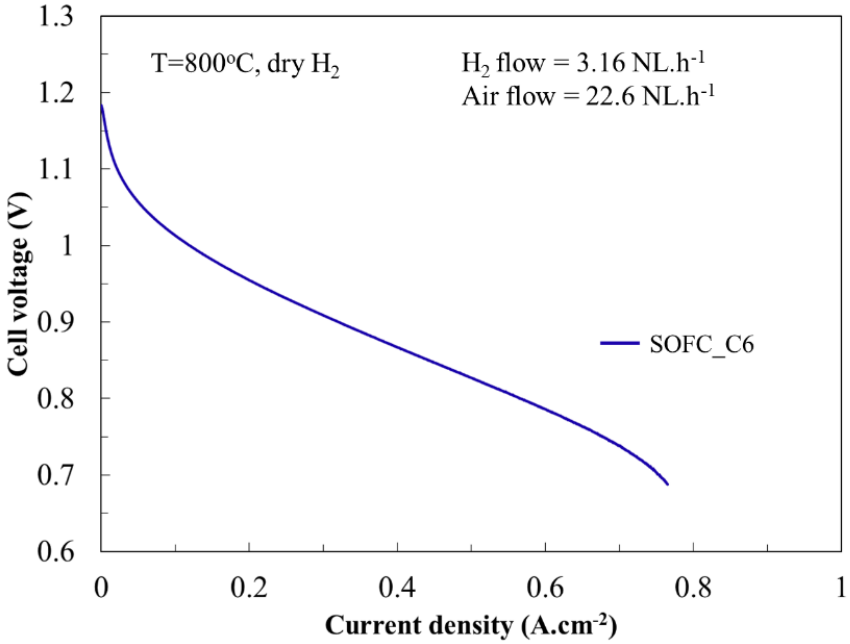

Figure 4.4, a typical cell polarisation curve is presented. As a general matter, the characteristics of the i-U curve given in

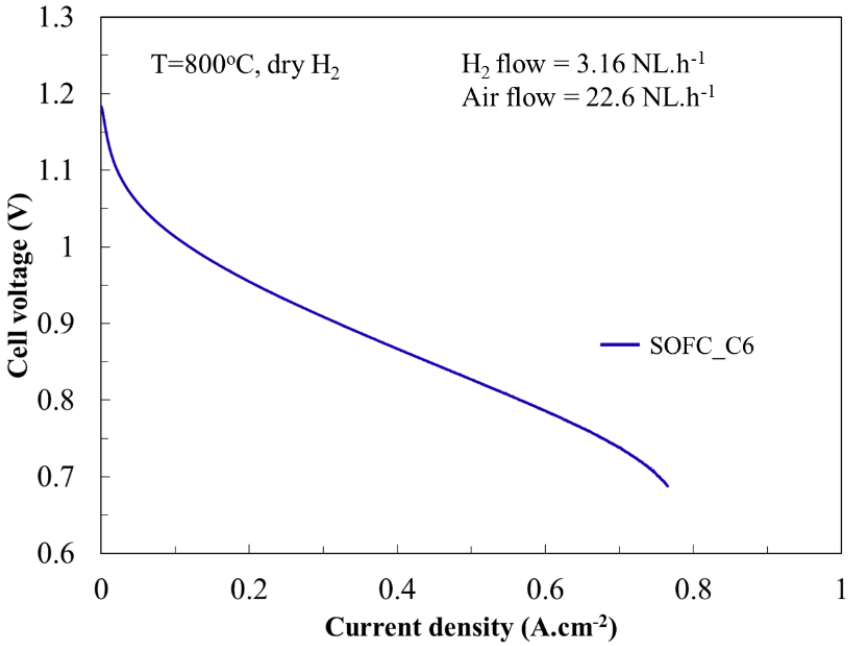

Figure 4.4 is found to be consistent with the ones expected for this kind of cells [Wuillemin2014]. This result allows validating the start-up protocol (heating, cermet reduction…) and the experimental set-up regarding the test performance. Moreover, the cells exhibit quite good performances meaning that they are well representative of the classical SOEC/SOFC technology.

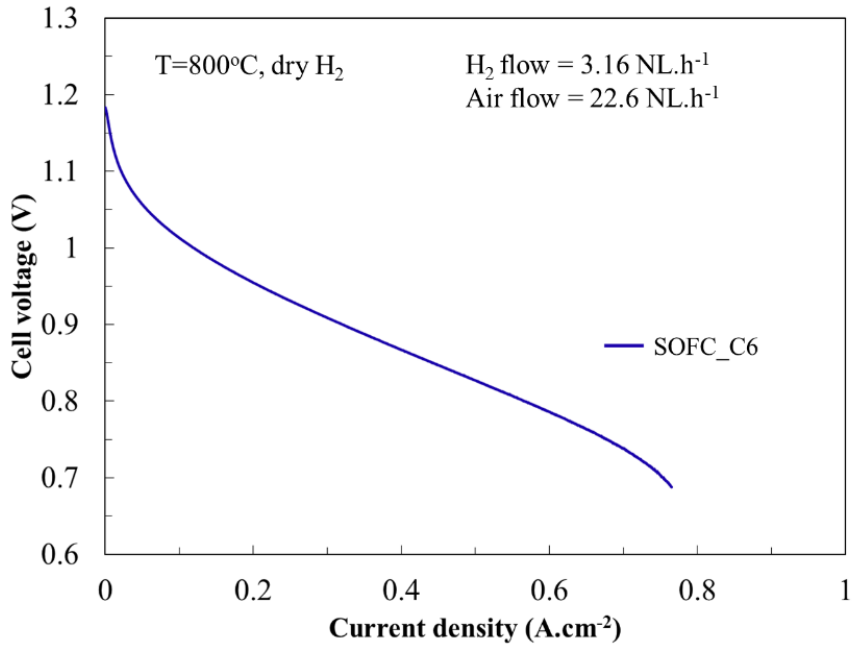

Figure 4.4 – Initial polarization curve in fuel cell mode of cell SOFC_C6 after cermet reduction at 800°C.

More precisely, the OCVs for the 6 tested cells are given in Table 4.1. As already stated, they are close to the theoretical value of 1.186 V (at 800°C for dry H_2 with 0.5% of residual steam) indicating a good cermet reduction and gas tightness of the anodic sealing. It can be mentioned that the cells from SOEC_C1 to SOFC_4 present a lower OCV than SOFC_5 and SOFC_6. That lower values are explained by a higher residual humidity in the inlet gas circuit (bubbler and buffer volume). By looking at the potential measured at 0.5 A.cm^{-2}, it can be seen that all the cells give a similar result (Table 4.1). The standard deviation on these measurements is about 8 mV. The ohmic resistance R_s given in Table 4.1 correspond to the electrolyte and contact resistance measured with EIS at 0.5 A.cm^{-2}. The cells SOFC_C5 and SOFC_C6 have a higher ohmic resistance since a lower mass pressure was applied in these cases (330 g.cm^{-2} instead of 400 g.cm^{-2}). All these results are in good agreement and valid the test bench reproducibility.

Table 4.1- Initial performances measures at 800°C under dry hydrogen for the tested cells.

Cell	OCV (A.cm^{-2})	U (@0.5 A.cm^{-2})	R_s (Ω.cm^2)
SOEC_C1	1.134	0.847	0.136
SOEC_C2	1.094	0.832	0.134
SOEC_C3	1.109	0.836	0.140
SOFC_C4	1.093	0.843	0.135
SOFC_C5	1.183	0.827	0.180
SOFC_C6	1.183	0.827	0.192

2.2 Durability tests

2.2.1 Test conditions

A set of long-term durability tests have been performed with different operating conditions. The experimental parameters have been selected to understand their effect on the degradation. All the experimental conditions are summarized in Table 4.2. The polarisation mode chosen for the ageing is indicated in the name of the sample. The green colours are related to cells tested in electrolysis whereas the blue colours test name are operated in fuel cell mode. Tests have been performed in galvanostatic condition at current densities varying between -0.5 A.cm^{-2} and -0.75 A.cm^{-2} in electrolysis and 0.5 A.cm^{-2} and 0.67 A. cm^{-2} in fuel cell mode. The temperature has been mainly set at 850°C to promote the degradation. One test was performed at 750°C to be able to identify the effect of this parameter on durability and microstructural evolutions.

Table 4.2 – Overview of tested cells operating conditions and ageing time

Test name	Temp. (°C)	H_2/H_2O	SC/FU (%)	*j* (A.cm^{-2})	Ageing time (h)
SOEC_C1	850	50/50	60	-0.5	1500
SOEC_C2	850	50/50	60	-0.5	2000
SOEC_C3	850	50/50	60	-0.75	2400
SOFC_C4	850	50/50	60	+0.5	1000
SOFC_C5	850	100/0	80	+0.66	1200
SOFC_C6	750	100/0	60	+0.5	9000

For all the tested cells, the air flow at the O_2 electrode has been adapted to keep an air conversion rate of 20%. This low value has been chosen to limit the oxygen partial pressure gradient along the cell radius. For the hydrogen electrode, four tests have been performed with a gas composition H_2/H_2O=50/50 and flow rates of 6.32 NL.h^{-1} (C1, C2 and C4) or 9.48 NL.h^{-1} (C3). This ratio allows the same OCP to be reached whatever the polarisation selected for the ageing. In other words, the effect of electrolysis or fuel cell mode could be analysed thanks to this composition. The two other tests were operated under dry hydrogen with a flow rate of 3.16 NL.h^{-1}. It should be noticed that all the experiments have been done over more than thousand hours.

2.2.2 Long-term tests

On Figure 4.5, the overpotential evolution over time is plotted for the cells aged with a ratio H_2/H_2O=50/50. The overpotential corresponds to the difference between the measured cell voltage in galvanostatic mode and the OCV. The absolute value of this parameter is considered to compare all the evolutions on the same graph whatever the polarisation (fuel cell or electrolysis). The initial points are different as the operating conditions changed according to the cells. It can be noticed that the curves are oscillating with an amplitude of about 20 mV in electrolysis and 5 mV in fuel cell mode during the test. This effect is directly linked to the humidifier which generates a non-perfectly continuous steam flow. This phenomenon has also been seen in other studies using bubbler or evaporator [Schefold2012, Schefold2015, Shimada2016]. A transient period of about 200h can be observed before a linear evolution of the cell overpotential. For all these cells, the overpotential evolution over time appears limited after the transient period.

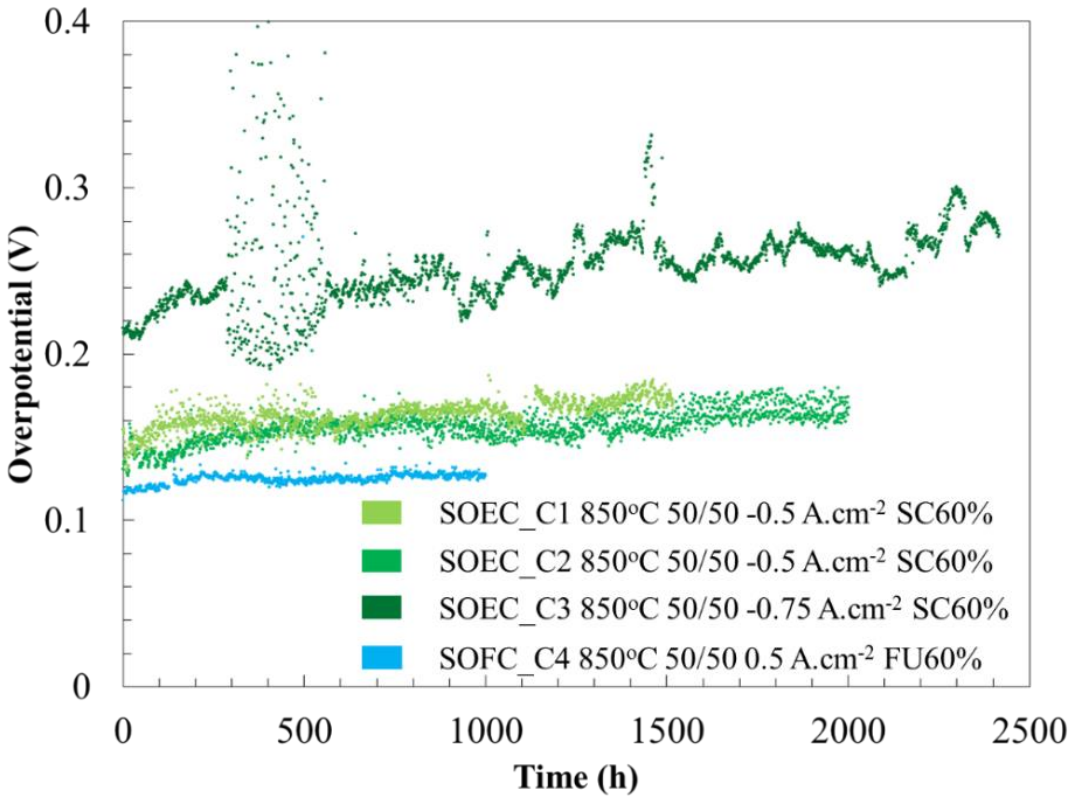

Figure 4.5 – Overpotential evolution over time for durability tests performed under H_2/H_2O=50/50. The overpotential is the absolute value of the difference between the cell potential and the OCV.

Other tests were performed in fuel cell mode under dry hydrogen atmosphere. Their overpotential evolutions are shown on Figure 4.6 with the cell SOFC_C4 previously presented. The initial overpotential values are higher as the OCV is higher under dry hydrogen. The cell SOFC_C5 presents a high degradation that could be due to the severe operating conditions chosen in that case. The last test SOFC_C6 was done in collaboration with B. Morel. This cell was aged at lower temperature (750°C) and during more than one year (9000h). Some test interruptions are visible but they are not detrimental for the cell life. A period of 300h at 80% FU is also observable after 1000h of ageing. It can be noticed that the overpotential evolution is not critically evolving during 9000h. The other tests stopped after a shorter time should be representative of the cell degradation over this long period of around 1 year.

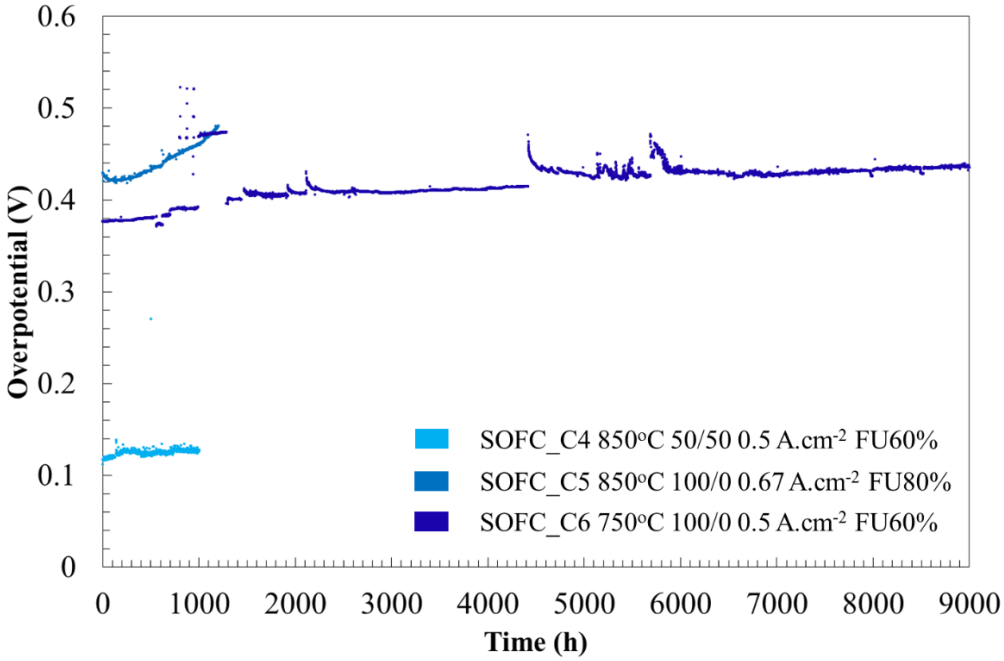

Figure 4.6 - Overpotential evolution over time for durability tests in fuel cell mode. The overpotential is the absolute value of the difference between the cell potential and the OCV.

2.2.3 Degradation rate results

For all the tested cells, the degradation rates have been measured after the transient period of ~200 hrs that is to say on the linear parts of the curve. The data are all summarised in Table 4.3. Note that for the cell SOFC_C6, two values of degradation rates are given. Indeed, two periods are visible on the curve plotted in Fig. 4.5. The first one lasted 2000h whereas the second one went to the end of the test with a lower degradation rate.

The uncertainties given for the degradation rates stem from the noise on the recorded raw data (see Figure 4.5 and Figure 4.6). It can be noticed that the degradation rates are very limited and are among the best results published in the literature, especially in SOEC mode [Schefold2015, The2015, Trofimenko2015].

Table 4.3 – Degradation rates measured on the total curve or linear part for the tested cells.

Test name	Degradation rate (mV.kh^{-1})	Degradation rate (%.kh^{-1})
SOEC_C1	9.7 ±2.0	0.90 ±0.2
SOEC_C2	8.8 ±1.0	0.84 ±0.1
SOEC_C3	15.8 ±3.0	1.39 ±0.3
SOFC_C4	3.5 ±1.0	0.43 ±0.1
SOFC_C5	57.2 ±2.0	6.96 ±0.2
SOFC_C6	(1) 13.5 ±0.5 (2) 4.1 ±1.0	(1) 1.64 ±0.1 (2) 0.50 ±0.1

From the degradation rate measurements, some discussions are possible on the "apparent" degradation of cells. The term "apparent" is specified to do the difference with the intrinsic degradation of cells. The following statements can be inferred from the degradations rates given in Table 4.3:

• SOEC_C1 and SOEC_C2 are performed in the same operating conditions. As expected, their degradations rates are found to be similar. It can thus be concluded that the durability tests are reproducible.

• The other test performed in electrolysis (SOEC_C3) presents a superior cell voltage evolution. In other words, it appears that the "apparent" degradation in electrolysis mode is more pronounced with a higher current density. This result is consistent and confirmed by many studies already reported in fuel cell mode [Hagen2006, Zhang2013b, Sun2015].

• The cell SOFC_C4 was tested in fuel cell mode with comparable test conditions than cell SOEC_C1 and SOEC_C2 in terms of temperature, inlet gas compositions and current density. It is found that the "apparent" degradation is clearly lower in fuel cell mode than in electrolysis mode. This statement indicates that an operation under electrolysis current is liable to induce larger deteriorations in the cell layers. This result is found to be in good agreement with the study of Zhang et al. [Zhang2013b] dedicated to the durability evaluation of reversible solid oxide cells.

• As expected, the cell SOFC_C5 aged with the most severe operating conditions, that is to say at the highest fuel utilisations (80%), exhibits the highest degradation rate. As for the effect of current density parameter, this result means that the highest is the fuel utilisation, the highest would be the "apparent" degradation rate. This statement has been already reported in many studies performed in fuel cell mode [Koch2006, Yokokawa2008]. Nevertheless, in our case, it is suspected that the very high degradation rates measured at 80% could be related to a non-homogeneous gas distribution on the electrode surface. Indeed, in this case, some part of the cell surface could be operated at fuel utilisation approaching or even exceeding 100%. This local over-fuel utilisation should accelerate the material degradation, and hence, should explain the rather high performance loss reported in Table 4.3 for SOFC_C5.

• The last durability experiment SOFC_C6 presents a rather low degradation rate over a period of more than 1 year. It worth reminding that this test was performed at a lower temperature than the others (i.e. 750°C instead of 850°C). However, despite a lower operating temperature, the "apparent" degradation rate is found to be slightly higher to the one obtained in similar conditions but at higher temperature (see degradation rate for SOFC_C4 operated at 850°C, 0.5A.cm^{-2} and FU=60%). This unexpected result has been already reported by other authors [Hagen2006, Diethelm2013, Fang2015, Kotisaari2016] and is still not understood.

All these results have shown effects of operating parameters on the "apparent" degradation. It is necessary to use other characterization techniques to analyse more finely the "intrinsic" cell degradation.

3. Conclusions

The experimental set-up detailed in this chapter was used to perform six different durability tests in galvanostatic mode over periods of more than 1000h. The effect of operating conditions on cell degradation have been highlighted by changing the polarisation, the current density and the temperature between the experiments. The degradations measured on cell voltage evolutions are in the state-of-the-art of the literature for both polarisations. It appears that the degradation rate is higher in electrolysis than in fuel cell mode for similar operating conditions. A higher current density also leads to a higher "apparent" degradation of the cell.

4. Bibliography

[Aaberg1998] R. J. Aaberg, R. Tunold, M. Mogensen, R. W. Berg, R. Ødegaård, "Morphological Changes at the Interface of the Nickel-Yttria Stabilized Zirconia Point Electrode", Journal of The Electrochemical Society 145(7) (1998) 2244-2252

[Barsoukov2005] E. Barsoukov, J. Ross Macdonald, eds. "Impedance spectroscopy: theory, experiment, and applications", John Wiley & Sons (2005)

[Diethelm2013] S. Diethelm, J. Van Herle, D. Montinaro, O. Bucheli, "Electrolysis and Co-Electrolysis Performance of SOE Short Stacks", Fuel Cells 13(4) (2013) 631-637

[Fang2015] Q. Fang, L. Blum, N. H. Menzler, "Performance and Degradation of Solid Oxide Electrolysis Cells in Stack", Journal of The Electrochemical Society 162(8) (2015) F907-F912

[Fergus2005] J. W. Fergus, "Metallic interconnects for solid oxide fuel cells", Materials Science and Engineering A397(1) (2005) 271-283

[Ghezel2013] H. Ghezel-Ayagh, "Advances in SOFC Development at FuelCell Energy ", 14th Annual SECA Workshop Pittsburgh (2013)

[Hagen2006] A. Hagen, R. Barfod, P. V. Hendriksen, Y.-L. Liu, S. Ramousse, "Degradation of anode supported SOFCs as a function of temperature and current load", Journal of the Electrochemical Society 153(6) (2006) A1165-A1171

[Hauch2011] A. Hauch, M. Mogensen, A. Hagen, "Ni/YSZ electrode degradation studied by impedance spectroscopy—Effect of p (H 2 O)", Solid State Ionics 192(1) (2011) 547-551

[Holzer2011] L. Holzer, B. Iwanschitz, T. Hocker, B. Münch, M. Prestat, D. Wiedenmann, U. Vogt, P. Holtappels, J. Sfeir, A. Mai, T. Graule, "Microstructure degradation of cermet anodes for solid oxide fuel cells: Quantification of nickel grain growth in dry and in humid atmospheres", Journal of Power Sources 196(3) (2011) 1279-1294

[Jia2006] L. Jia, Z. Lu, J. Miao, Z. Liu, G. Li, W. Su, "Effects of pre-calcined YSZ powders at different temperatures on Ni–YSZ anodes for SOFC", Journal of alloys and compounds 414(1) (2006) 152-157

[Jiang1999] S. P. Jiang, S. P. S. Badwal, "An electrode kinetics study of H 2 oxidation on Ni/Y 2 O 3–ZrO 2 cermet electrode of the solid oxide fuel cell", Solid State Ionics 123(1) (1999) 209-224

[Jiang2003] S. P. Jiang, "Sintering behavior of Ni/Y2O3-ZrO2cermet electrodes of solid oxide fuel cells", Journal of materials science 38(18) (2003) 3775-3782

[Koch2006] S. Koch, P. V. Hendriksen, M. Mogensen, Y-L. Liu, N. Dekker, B. Rietveld, B. De Haart, F. Tietz, "Solid oxide fuel cell performance under severe operating conditions", Fuel Cells 6(2) (2006) 130-136

[Kotisaari2016] M. Kotisaari, O. Thomann, D. Montinaro, J. Kiviaho, "Evaluation of a SOEC stack for hydrogen and syngas production: a performance and durability analysis", 12th European SOFC & SOE Forum Lucerne (2016) A1202

[Lay2013] E. Lay-Grindler, J. Laurencin, J. Villanova, I. Kieffer, F. Usseglio-Viretta, T. Le Bihan, P. Bleuet, A. Mansuy, G. Delette, "Degradation study of the La0. 6Sr0. 4Co0. 2Fe0. 8O3 solid oxide electrolysis cell (SOEC) anode after high temperature electrolysis operation", ECS Transactions 57(1) (2013) 3177-3187

[Matsui2012] T. Matsui, R. Kishida, H. Muroyama, K. Eguchi, "Comparative Study on Performance Stability of Ni–Oxide Cermet Anodes under Humidified Atmospheres in Solid Oxide Fuel Cells", Journal of The Electrochemical Society 159(8) (2012) F456-F460

[Mogensen2016] M. B. Mogensen, A. Hauch, X. Sun, M. Chen, Y. Tao, S. D. Ebbesen, P. V. Hendriksen, "Relation between shape of Ni-particles and Ni migration in Ni-YSZ electrodes–a hypothesis", In Proceedings of the 12th European Sofc & Soe Forum, European Fuel Cell Forum, (2016)

[Nechache2014] A. Nechache, M. Cassir, A. Ringuedé, "Solid oxide electrolysis cell analysis by means of electrochemical impedance spectroscopy: A review", Journal of Power Sources 258 (2014) 164-181

[Park2010] K. Park, S. Yu, J. Bae, H. Kim, Y. Ko, "Fast performance degradation of SOFC caused by cathode delamination in long-term testing", international journal of hydrogen energy 35(16) (2010) 8670-8677

[Pihlatie2011] M. H. Pihlatie, A. Kaiser, M. Mogensen, M. Chen, "Electrical conductivity of Ni–YSZ composites: Degradation due to Ni particle growth", Solid State Ionics 189(1) (2011) 82-90

[Rinaldi2015] L. Rinaldi, "XX", Master thesis University of Salerno (2015)

[Schefold2012] J. Schefold, A. Brisse, F. Tietz, "Nine thousand hours of operation of a solid oxide cell in steam electrolysis mode", Journal of The Electrochemical Society 159(2) (2011) A137-A144

[Schefold2015] J. Schefold, A. Brisse, H. Poepke, "Long-term Steam Electrolysis with Electrolyte-Supported Solid Oxide Cells", Electrochimica Acta 179 (2015) 161-168

[Schuler2012] J. A. Schuler, Z. Wuillemin, A. Hessler-Wyser, C. Comminges, N. Y. Steiner, J. Van Herle, "Cr-poisoning in (La, Sr)(Co, Fe) O 3 cathodes after 10,000 h SOFC stack testing", Journal of Power Sources 211 (2012) 177-183

[Shimada2016] H. Shimada, T. Yamaguchi, T. Suzuki, H. Sumi, K. Hamamoto, Y. Fujishiro, "High steam utilization operation with high current density in solid oxide electrolysis cells", Journal of the Ceramic Society of Japan 124(3) (2016) 213-217

[Sun2015] X. Sun, M. Chen, Y.-L. Liu, P. V. Hendriksen, "Life Time Performance Characterization of Solid Oxide Electrolysis Cells for Hydrogen Production", ECS Transactions 68(1) (2015) 3359-3368

[The2015] D. The, S. Grieshammer, M. Schroeder, M. Martin, M. Al Daroukh, F. Tietz, J. Schefold, A. Brisse, "Microstructural comparison of solid oxide electrolyser cells operated for 6100 h and 9000 h", Journal of power sources 275 (2015) 901-911

[Trofimenko2015] N. Trofimenko, M. Kusnezoff, D. Klemm, D. Schimanke, "Development of Electrolyte Supported Cells Based on a Thin 3YSZ Substrate: Through Optimized Contact Layer to High Power Density", ECS Transactions 68(1) (2015) 1933-1942

[Tu2004] H. Tu, U. Stimming, "Advances, aging mechanisms and lifetime in solid-oxide fuel cells", Journal of Power Sources 127(1) (2004) 284-293

[Wang2016] H. Wang, K. J. Yakal-Kremski, T. Yeh, G. M. Rupp, A. Limbeck, J. Fleig, S. A. Barnett, "Mechanisms of Performance Degradation of (La, Sr)(Co, Fe) O3-δ Solid Oxide Fuel Cell Cathodes", Journal of The Electrochemical Society 163(6) (2016) F581-F585

[Wuillemin2014] Z. Wuillemin, S. Ceschini, Y. Antonetti, C. Beetschen, S. Modena, D. Montinaro, T. Cornu, O. Bucheli, M. Bertoldi, “High-performance SOFC stacks tested under different reformate compositions”, 11th European SOFC & SOE Forum Lucerne (2014) A0901

[Yokokawa2008] H. Yokokawa, H. Tu, B. Iwanschitz, A. Mai, "Fundamental mechanisms limiting solid oxide fuel cell durability", Journal of Power Sources 182(2) (2008) 400-412

[Zhang2013] X. Zhang, J. E. O'Brien, R. C. O'Brien, J. J. Hartvigsen, G. Tao, G. K. Housley, "Improved durability of SOEC stacks for high temperature electrolysis", International Journal of Hydrogen Energy 38(1) (2013) 20-28

[Zhang2013b] X. Zhang, J. E. O'Brien, R. C. O'Brien, G. K. Housley, "Durability evaluation of reversible solid oxide cells", Journal of Power Sources 242 (2013) 566-574

[Zhu2003] W. Z. Zhu, S. C. Deevi, "A review on the status of anode materials for solid oxide fuel cells", Materials Science and Engineering: A 362(1) (2003) 228-239